arXiv:cond-mat/0103368v1 [cond-mat.stat-mech] 17 Mar 2001

Discrete Solitons and Breathers with Dilute Bose-Einstein Condensates

Andrea Trombettoni and Augusto Smerzi

Istituto Nazionale di Fisica per la Materia and International School for Advanced Studies, via Beirut 2/4, I-34014, Trieste, Italy

(February 1, 2008)

Abstract

We study the dynamical phase diagram of a dilute Bose-Einstein condensate (BEC) trapped in a periodic potential. The dynamics is governed by a discrete non-linear Schrödinger equation: intrinsically localized excitations, including discrete solitons and breathers, can be created even if the BEC's interatomic potential is repulsive. Furthermore, we analyze the Anderson-Kasevich experiment [Science **282**, 1686 (1998)], pointing out that mean field effects lead to a coherent destruction of the interwell Bloch oscillations.

PACS: 63.20.Pw, 05.45.-a

Typeset using REVTEX

Localization phenomena are ubiquitous in physics and in biology [1]. Intrinsically localized excitations, as solitons (shape preserving) and breathers (characterized by internal oscillations), are important channels for energy transport in non-linear media, such as optical fibres and waveguides [2], polaronic materials [3] and biological molecules [4]. Intense theoretical research is now focusing on the existence of solitons and breathers in a lattice (often named discrete solitons and discrete breathers (DSB) [2]), such as those appearing in quantum systems governed by a discrete non-linear Schrödinger equation (DNLSE) [5–7]. Current approaches include the search for exact solutions in some limits [8]; effective (point) particle and variational approaches [9–11]; perturbation around the linearized case and, of course, numerical solutions [2,5]. Although intensely studied, DSB have been experimentally observed only quite recently in superconducting ladders of Josephson junctions [12], in antiferromagnet systems [13], in optical waveguides [14] and in low dimensional materials [15].

The discrete solitons/breathers are characterized by a dynamical, self-maintained energy localization, due to both the discreteness and the non-linearity of the underlying equations of motion. The discreteness provides a band structure of the excitation spectrum, while the non-linearity allows for the tuning of the DSB energy outside the band. The finite energy gap guarantees the (meta-)stability of the DSB's. These, obviously, have a different nature to the "Anderson localizations", created by impurities or imperfections of the lattice [16]; the incorporation of disorder into non-linear excitations, and the tracing out of its dynamical effects are also important theoretical problems.

Bright solitons can occur in spatially homogeneous, dilute Bose-Einstein condensates (BEC) with an attractive interatomic interaction (s-wave scattering length $a < 0$) [17,18]. Dark solitons, propagating density dips, have been predicted and experimentally observed in BEC's with a repulsive interaction ($a > 0$) [19]. The dynamics of a BEC trapped in a spatially periodic potential [20–22], on the other hand, can be mapped, in the tight binding approximation, to a DNLSE. Bright discrete solitons and breathers can be created in DNLSE even with a repulsive BEC interatomic interaction.

In Ref. [23] a one-dimensional, vertical optical array was created by two counterpropagating laser beams. A weakly interacting Bose-Einstein condensate was trapped in ~ 30 wells, situated at the antinodes of the standing optical wave. Each well contained approximately 1000 condensate atoms, with the peak densities matching a gaussian profile. The lowest Bloch band dynamics of this system maps on a DNLSE, obtained by discretizing the Gross-Pitaevskii equation governing the condensate dynamics in the periodic potential. Since the array is oriented vertically, the atoms undergo coherent Bloch oscillations, driven by the interwell gravitational potential. At the edge of the Brillouin zone, a fraction of atoms can Zener tunnel in the higher energy band which, in this specific case, is in the continuum. A coherent leakage from the trap was observed at each Bloch period. However, an increase of the on-site particle densities washed out the coherent signal. This has been understood as a drift of the relative phases between wells due to mean field effects [23].

In this Letter we study the DNLSE using a variational approach: we show that a (complex) gaussian variational ansatz (describing a soliton / breather profile, combined with a Lagrangian optimization) yields a coupled dynamics of the profile parameters. A variety of discrete solitons / breathers are investigated analytically and compared with numerical calculations. This comparison is surprisingly successful in describing even details of the quite complex dynamical and collisional behaviour. Stability phase diagrams for such states are obtained by inspection of the profile dynamics equations.

The full Bose condensate dynamics satisfies the Gross-Pitaevskii equation (GPE) [24]:

$$i\hbar\frac{\partial\Phi}{\partial t} = -\frac{\hbar^2}{2m}\nabla^2\Phi + [V_{ext} + g_0 \mid \Phi \mid^2]\Phi \tag{1}$$

where V_{ext} is the external potential and $g_0 = \frac{4\pi\hbar^2 a}{m}$, with m the atomic mass. For a tilted trap as in [23] the external potential is given by the sum of the gravitational potential and the laser field

$$V_{ext}(\vec{r}) = mgz + U_L(x,y)\sin^2[2\pi z/\lambda] \tag{2}$$

where λ is the wavelength of the lasers (the spacing in the lattice is $\lambda/2$) and $U_L(x,y)$ is determined by the transverse intensity profile of the (nearly gaussian) laser beams. In [23]

$\lambda = 850$ nm and the $1/e^2$ radius of the transverse profile is $\approx 80\mu$m, an order of magnitude larger than the transverse radius of the condensate. The well depths scale linearly with the intensity of the beam. At the center of the beam the trap depths are $1.4E_R$ where $E_R = \frac{\hbar^2 k^2}{2m}$ is the recoil energy ($k = \frac{2\pi}{\lambda}$).

In the tight-binding approximation the condensate order parameter can be written as:

$$\Phi(\vec{r}, t) = \sqrt{N_T} \sum_n \psi_n(t)\ \phi(\vec{r} - \vec{r}_n), \tag{3}$$

where N_T is the total number of atoms and $\phi(\vec{r} - \vec{r}_n)$ is the condensate wave function localized in the trap n with $\int d\vec{r}\ \phi_n\ \phi_{n+1} \simeq 0$, and $\int d\vec{r}\ \phi_n^2 = 1$. $\psi_n = \sqrt{\rho_n(t)}\, e^{i\theta_n(t)}$ is the n-th amplitude ($\rho_n = N_n/N_T$, where N_n and θ_n are the number of particles and phases in the trap n). Replacing the ansatz (3) in (1) we find that the GPE reduces to a DNLSE:

$$i\frac{\partial \psi_n}{\partial t} = -\frac{1}{2}(\psi_{n-1} + \psi_{n+1}) + (\epsilon_n + \Lambda \mid \psi_n \mid^2)\psi_n \tag{4}$$

where $\epsilon_n = \frac{1}{2K}\int d\vec{r}[\frac{\hbar^2}{2m}(\vec{\nabla}\phi_n)^2 + V_{ext}\phi_n^2]$, $\Lambda = \frac{g_0 N_T}{2K}\int d\vec{r}\,\phi_n^4$ and $K \simeq -\int d\vec{r}[\frac{\hbar^2}{2m}\vec{\nabla}\phi_n \cdot \vec{\nabla}\phi_{n+1} + \phi_n V_{ext}\phi_{n+1}]$; the time has been rescaled as $t \rightarrow \frac{\hbar}{2K}t$. Eq. (4) is the equation of motion $\dot{\psi_n} = \frac{\partial \mathcal{H}}{\partial(i\psi_n^*)}$, where $\mathcal{H}$ is the Hamiltonian function

$$\mathcal{H} = \sum_n [-\frac{1}{2}(\psi_n \psi_{n+1}^* + \psi_n^* \psi_{n+1}) + \epsilon_n \mid \psi_n \mid^2 + \frac{\Lambda}{2} \mid \psi_n \mid^4] \tag{5}$$

with $i\psi_n^*, \psi_n$ canonically conjugate variables. Both the Hamiltonian $\mathcal{H}$ and the norm $\sum_n \mid \psi_n \mid^2 = 1$ are conserved.

To analyze the Anderson-Kasevich experiment, we study the dynamical evolution of a gaussian profile wave packet, which we parametrize as $\psi_V^n(t) = \sqrt{k} \cdot \exp\Big\{ -\frac{(n-\xi)^2}{\gamma^2} + ip(n-\xi) + i\frac{\delta}{2}(n-\xi)^2 \Big\}$ where $\xi(t)$ and $\gamma(t)$ are, respectively, the center and the width (in the lattice units) of the density $\rho_n = \mid \psi_n \mid^2$, $p(t)$ and $\delta(t)$ their associated momenta and $k(\gamma, \xi)$ a normalization factor. The wave packet dynamical evolution can be obtained by a variational principle from the Lagrangian $\mathcal{L} = \sum_n i\dot{\psi}_n \psi_n^* - \mathcal{H}$, with the equations of motion for the variational parameters $q_i(t) = \xi, \gamma, p, \delta$ given by $\frac{d}{dt}\frac{\partial \mathcal{L}}{\partial \dot{q}_i} = \frac{\partial \mathcal{L}}{\partial q_i}$. After some algebra we obtain [25] $\mathcal{L} = p\dot{\xi} - \frac{\gamma^2\dot{\delta}}{8} - \frac{\Lambda}{2\sqrt{\pi}\gamma} + \cos p \cdot e^{-\eta} - V(\gamma, \xi)$ where $\eta = \frac{1}{2\gamma^2} + \frac{\gamma^2\delta^2}{8}$ and $V = k \int\limits_{-\infty}^{\infty} dn\, \epsilon_n e^{-\frac{2(n-\xi)^2}{\gamma^2}}$. The variational equations of motion become:

$$\begin{cases} \dot{p} = -\frac{\partial V}{\partial \xi} \\ \dot{\xi} = \sin p \cdot e^{-\eta} \end{cases} \tag{6}$$

$$\begin{cases} \dot{\delta} = \cos p \Big(\frac{4}{\gamma^4} - \delta^2 \Big) e^{-\eta} + \frac{2\Lambda}{\sqrt{\pi}\gamma^3} - \frac{4}{\gamma} \frac{\partial V}{\partial \gamma} \\ \dot{\gamma} = \gamma \delta \cos p \cdot e^{-\eta} \end{cases} \tag{7}$$

with the pairs ξ, p and $\frac{\gamma^2}{8}, \delta$ which are canonically conjugate dynamical variables with respect to the effective Hamiltonian

$$H = \frac{\Lambda}{2\sqrt{\pi}\gamma} - \cos p \cdot e^{-\eta} + V(\gamma, \xi). \tag{8}$$

The wave packet group velocity is given by $v_g \equiv \frac{\partial H}{\partial p} = \dot{\xi} = \tan p / m^*$ with an inverse effective mass $(m^*)^{-1} \equiv \frac{\partial^2 H}{\partial p^2} = \cos p \, e^{-\eta}$. The quasi-momentum dependence of the effective mass allows a rich variety of dynamical regimes. Solitonic solutions with a positive non-linear parameter $\Lambda > 0$, for instance, are allowed by a negative effective mass. A regime with a diverging effective mass $m^* \to \infty$ leads to a self-trapping of the wave packet.

In the following we will study the dynamical regimes of Eq. (4) in two particular cases. We first consider a tilted (washboard) periodic potential describing the vertical optical trap created in the Anderson-Kasevich experiment. In particular, we will show that non-linear effects tend to destroy the Bloch oscillations, consistently with the experimental results. The external potential for the tilted trap is given by Eq. (2) with $\epsilon_n = \omega n$ where $\omega = \frac{mg\lambda/2}{2K}$. We find $V = \omega \xi$ and $\dot{p} = -\omega$ [26].

Then we consider the case of an horizontal array, in which gravitation only provides a constant energy shift, with $\dot{p} = 0$. We will classify four different regimes which include discrete breathers and solitons.

Tilted trap. It is well known that single atoms in a tilted washboard potential oscillate among sites at the Bloch frequency. This regime is described by Eqs. (6, 7) with $\Lambda = 0$ (corresponding to a negligible mean field condensate interaction). This is, precisely, the regime investigated in [23] in which a coherent output was observed. Indeed a variational estimate gives $\Lambda \simeq 0.5$ and $\omega \simeq 2$ (the scaled time is in units of

$\hbar/2K = 0.35ms$). In this limit the equations of motion can be solved exactly giving $p(t) = -\omega t + p_0$, $\xi(t) = -A[\cos p_0 - \cos(\omega t - p_0)]$, $\gamma^2(t) = 4A^2 \log A\omega\{\cos[2(\omega t - p_0)] - \cos 2p_0 - 4\sin p_0 \sin(\omega t - p_0) - 4\sin^2 p_0\} + \gamma_0^2$ and $\delta(t) = -\frac{8A \log A\omega [\sin(\omega t - p_0) + \sin p_0]}{\gamma^2(t)}$ where $A = -H_0/\omega \cos p_0$, $\delta(0) = \delta_0 = 0$ and H_0 is the (conserved) initial energy. In the inset of Fig. 1 we show that the Bloch oscillations described by the variational ansatz (solid line) are in excellent agreement with the full numerical solution of the DNLSE (dashed line). The numerical average position is defined as $\sum_n n \mid \psi_n \mid^2$.

The effect of non-linearity on the Bloch oscillations is dramatic. This has been studied experimentally in [23] by increasing the density in each well, and observing a degradation in the interference pattern. With $\Lambda \neq 0$ we have:

$$\ddot{\xi} + \frac{\Lambda\delta}{2\sqrt{\pi}\gamma}\dot{\xi} + \omega^2\xi = \omega H_0 - \frac{\Lambda\omega}{2\sqrt{\pi}\gamma}. \tag{9}$$

The Eq. (9) displays an effective damping term proportional to the velocity $\dot{\xi}$. We stress that the dynamics is fully Hamiltonian, and real dissipative processes are absent. For $t \to \infty$, γ tends to a constant value γ_{fin} and $\delta \sim \frac{2\Lambda}{\sqrt{\pi}\gamma_{fin}^3}t$, so the term $\Lambda\delta$ has the correct positive sign (for large t). The apparent damping is the consequence of a diverging effective mass of the wave packet $m^* \sim e^{\frac{\Lambda^2}{2\pi\gamma_{fin}^4}t^2}$, which stops the Bloch oscillations. This effect manifests, in the numerical analysis of Eq. (4), as a distortion of the on-site phases. In Fig.1 (solid line) we show the variational Bloch dynamics with a non-linear parameter $\Lambda = 10$ and initial values $\xi_0 = 0$, $p_0 = 0$ and $\delta_0 = 0$. The oscillation roughly decreases as $\xi(t) \sim -A(1 - e^{-\frac{\Lambda^2 t^2}{2\pi\gamma_{fin}^4}} \cos\omega t)$. The dashed line shows the full numerical solution of the DNLSE, in good agreement with the analytical result (solid line). The discrepancy at $t > 10$ is due to the breaking of the gaussian wave packet in the numerical simulation.

Untilted trap. The momentum $p(t) = p_0$ is conserved. We note that the equations of motion are invariant with respect to the replacement $\Lambda \to -\Lambda$, $p_0 \to p_0 + \pi$ and $t \to -t$. In Fig. 2 we report the dynamical phase diagram as a function of Λ versus $\cos p$, for $\Lambda > 0$ and with initial values $\xi_0 = 0$ and $\delta_0 = 0$. This phase diagram has been calculated analytically from Eqs. (6-8) and checked numerically. In the region $\cos p > 0$ there are two

distinct regimes. When $H_0 > 0$, $\gamma(t) < \gamma_{max}$: this is the self-trapped regime in which the boson wave packet remains localized around few sites. The self-localization is a genuine non-linear effect, characterized by a diverging effective mass. In particular, the self-trapped wave packet cannot translate along the array: this is a major difference with respect to soliton-like solutions. The limit values for $t \to \infty$ are $\gamma \to \frac{\Lambda}{2\sqrt{\pi}H_0}$, $\delta \to \infty$ and $\dot{\xi} \to 0$. We note that a non-linear self-trapping occurs also in a two-site problem [27].

A diffusive regime occurs when $-\cos p_0 < H_0 \leq 0$. In this case $\gamma(t \to \infty) \to \infty$ and $\dot{\xi} \approx -H_0/\tan p_0 = const.$ The transition between the two regimes occurs at $\Lambda_c = 2\sqrt{\pi}\,\gamma_0 \cos p_0\, e^{-1/2\gamma_0^2}$. With $\Lambda > \Lambda_c$, the ratio between the initial value of the width γ_0 and the limit width $\gamma_{max}(t \to \infty)$ is given by

$$\frac{\gamma_0}{\gamma_{max}} = \frac{\Lambda - \Lambda_c}{\Lambda}. \tag{10}$$

In Fig. 3 we plot γ_0/γ_{max} vs. Λ/Λ_c while in the inset we report the variational and numerical values of the width of the density vs. Λ/Λ_c after a time $\tau = 10$ (scaled units). The discrepancy at large Λ/Λ_c is due to a slight deviation of the numerical density profile from a gaussian shape. We checked the stability of self-trapping, also considering different initial forms of the wave packet.

In the region $\cos p < 0$ the self-trapping condition is given by $H_0 > \mid \cos p_0 \mid$: in this case $\Lambda_c = 2\sqrt{\pi}\,\gamma_0 \mid \cos p_0 \mid\ (1 - e^{-1/2\gamma_0^2})$. A soliton solution can be determined by imposing $\dot{\gamma} = \dot{\delta} = 0$. We find $\Lambda_{sol} = 2\sqrt{\pi}\frac{|\cos p_0|}{\gamma_0}\, e^{-1/2\gamma_0^2}$. For $\Lambda = \Lambda_{sol}$ the center of the wave packet moves with a constant velocity $\dot{\xi}$ and its width remains constant in time. For $\Lambda_c < \Lambda < \Lambda_{sol}$, $\xi \to \infty$ while $\gamma(t)$ oscillates, corresponding to a breather solution. The numerical solution of Eq. (4) confirms the variational predictions. In Fig. 4(a) we report the numerical density profile for Λ in the breather region with $p_0 = 3\pi/4$; in Fig. 4(b) the numerical density profile is drawn for the same Λ and $p_0 = \pi/4$: the change of the sign of $\cos p$ gives a breather solution in the first case, and the spreading of the density in the second one. In Figs. 4(c) and 4(d) we show that for $\Lambda = \Lambda_{sol}$ the soliton after hitting a wall rebounds and regains its shape.

In conclusion, we have studied the dynamics of a dilute Bose condensate trapped in a periodic potential. We have analyzed the Anderson-Kasevich experiment, pointing out that mean field effects lead to a coherent destruction of the interwell Bloch oscillations. We have shown that intrinsically localized excitations, like discrete breathers and solitons, can exist also with a repulsive interatomic potential by studying analytically their dynamical phase diagram.

Discussions with S.R. Shenoy and P. Sodano are acknowledged. This work has been supported by the Cofinanziamento MURST.

REFERENCES

[1] *Proceedings of the Conference on Future Directions of Nonlinear Dynamics in Physical and Biological Systems, Denmark,* edited by P.L. Christiansen, J.C. Eilbeck, and R.D. Parmentier [Physica (Amsterdam) **68D**, 1-186 (1993)].

[2] S. Flach and C.R. Willis, Phys. Rep. **295**, 181 (1998).

[3] J.D. Andersen and V.M. Kenkre, Phys. Rev. **B47**, 11134 (1993).

[4] M. Peyrard *et al.*, Physica **68D**, 104 (1993).

[5] D. Hennig and G.P. Tsironis, Phys. Rep. **307**, 333 (1999).

[6] K.O. Rasmussen, T. Cretegny, P.G. Kevrekidis, and N.G. Gronbech-Jensen, Phys. Rev. Lett. **84**, 3740 (2000).

[7] P.G. Kevrekidis, K.O. Rasmussen, and A.R. Bishop, Phys. Rev **E61**, 2652 (2000).

[8] D. Cai, A.R. Bishop, and N. Gronbech-Jensen, Phys Rev. Lett. **72**, 591 (1994); Phys. Rev. **E53**, 4131 (1996).

[9] R. Scharf and A.R. Bishop, Phys. Rev. **A43**, 6535 (1991); Phys. Rev. **E47**, 1375 (1993).

[10] F. Cooper, H. Shepard, C. Lucheroni, and P. Sodano, Physica **68D**, 344 (1993).

[11] A.B. Aceves *et al.*, Phys. Rev. **E53**, 1172 (1996).

[12] P. Binder *et al.*, Phys. Rev. Lett. **84**, 745 (2000); E. Trias *et al.*, Phys. Rev. Lett. **84**, 741 (2000).

[13] U.T. Schwarz, L.Q. English, and A.J. Sievers, Phys. Rev. Lett. **83**, 223 (1999).

[14] H.S. Eisenberg *et al.*, Phys. Rev. Lett. **81**, 3383 (1998).

[15] B.I. Swanson *et al.*, Phys. Rev. Lett. **82**, 3288 (1999).

[16] T.V. Ramakrishnan, in *Chance and Matter*, Proceedings of the Les Houches Summer

School, Session XLVI, edited by J. Souletie, J. Vannimenus, and R. Stora (North-Holland, Amsterdam, 1987), p. 213.

[17] D. Jaksch *et al.*, Phys. Rev. Lett. **81**, 3108 (1998).

[18] O. Zubay *et al.*, Phys. Rev. **A59**, 643 (1999).

[19] S. Burger *et al.*, Phys. Rev. Lett. **83**, 5198 (1999).

[20] K. Berg-Sorensen and K. Molmer, Phys. Rev. **A58**, 1480 (1999).

[21] J. Javanainen, Phys. Rev. **A60**, 4902 (1999).

[22] M.L. Chiofalo and M.P. Tosi, Phys. Lett. **A268**, 406 (2000).

[23] B.P. Anderson and M.A. Kasevich, Science **282**, 1686 (1998).

[24] F. Dalfovo, S. Giorgini, L.P. Pitaevskii, and S. Stringari, Rev. Mod. Phys. **71**, 463 (1999).

[25] With γ not too small ($\gamma > 1$) we can replace the sums over n in the Lagrangian with integrals: $\sum_{n=-\infty}^{\infty} e^{-\frac{(n-\xi)^2}{\gamma^2}} \Big/ \int_{-\infty}^{\infty} e^{-\frac{(n-\xi)^2}{\gamma^2}} dn = 1 + e^{-\pi^2\gamma^2} \cos(2\pi\xi) + O(e^{-4\pi^2\gamma^2})$. In this limit the normalization factor becomes $k = \sqrt{2/\pi\gamma^2}$.

[26] We note that for a quadratic potential $\epsilon_n = \Omega n^2$ we would have $V(\gamma, \xi) = \Omega(\xi^2 + \gamma^2/4)$ and $\dot{p} = -2\Omega\xi$.

[27] A. Smerzi *et al.*, Phys. Rev. Lett. **79**, 4950 (1997); S. Raghavan *et al.*, Phys. Rev. **A59**, 620 (1999).

FIGURES

FIG. 1. Coherent destruction of Bloch oscillations: numerical (dashed line) and variational (solid line) average position of the density in the tilted trap ($\omega = 2$, $\Lambda = 10$ and initial $p_0 = 0$, $\delta_0 = 0$, $\gamma_0 = 10$). Inset: Bloch oscillations for $\Lambda = 0$.

FIG. 2. Dynamical phase diagram in the untilted trap: Λ vs. $\cos p$, for $\Lambda > 0$ and with initial $\xi_0 = 0$ and $\delta_0 = 0$.

FIG. 3. Universal curve for γ_0/γ_{max} vs. Λ/Λ_c as in Eq. (10). The inset shows the variational (solid line) and numerical (circles) width of the density vs. Λ/Λ_c after the time $\tau = 10$, scaled units (initial values: $p_0 = 0$, $\delta_0 = 0$ and $\gamma_0 = 7$).

FIG. 4. (a) Numerical density profiles calculated at different times ($t = 0, 50, 100, \ldots, 400$). The value of Λ is inside the breather region of the dynamical phase diagram ($p_0 = 3\pi/4$, $\gamma_0 = 10$, $\Lambda = 0.24$); (b) the same parameters as in (a), but for $p_0 = \pi/4$; (c) width (dotted line) and average position (solid line) calculated numerically for $\Lambda = \Lambda_{sol}$ and $p_0 = 3\pi/4$ in a finite array of 73 sites (the soliton hits a wall); (d) numerical density profile for $t = 0, 50, 100, 150, 200$ for the soliton described in (c).

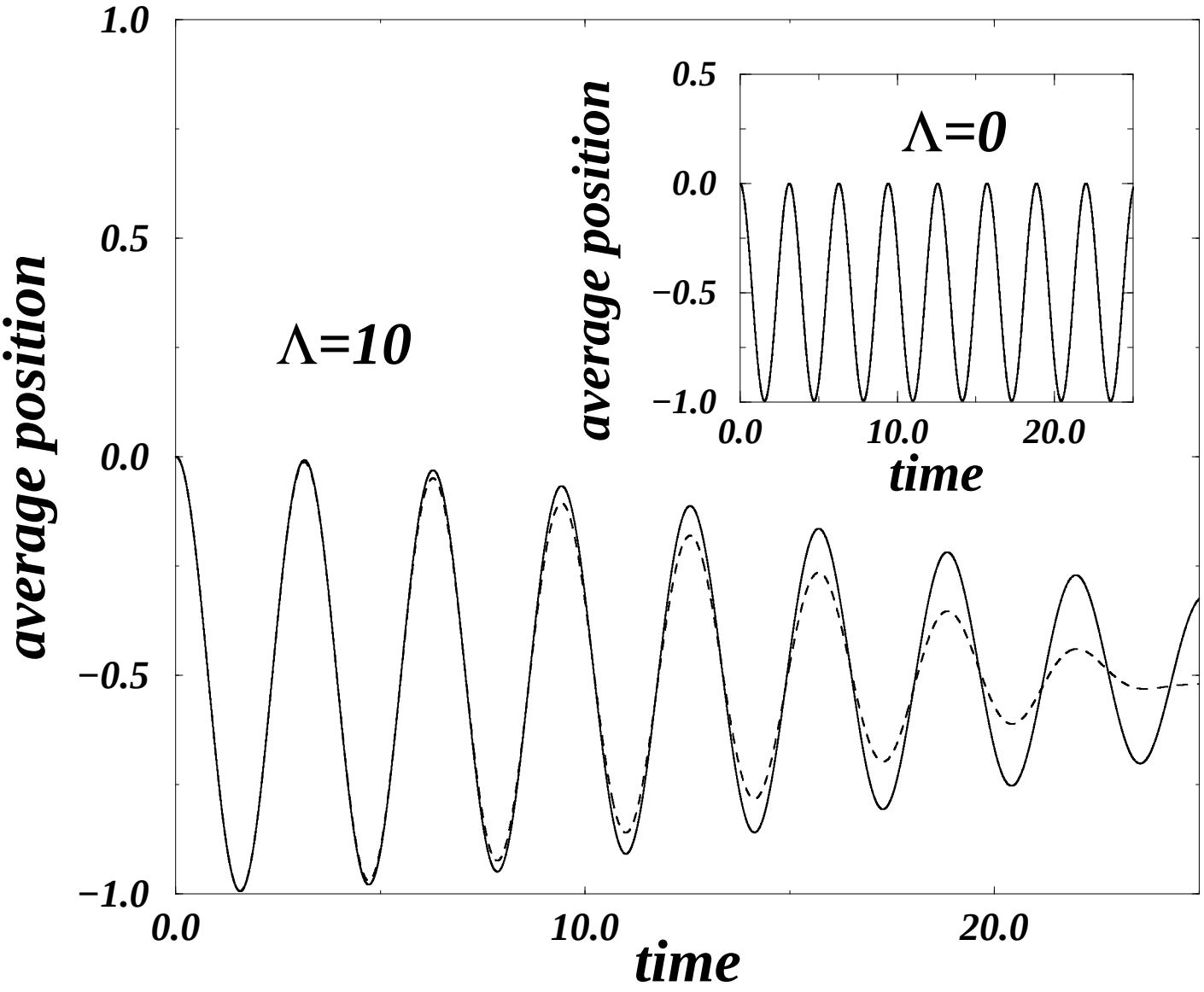
1.0
0.5
0.0
−0.5
−1.0
average position
Λ=10
0.0
10.0
20.0
time
0.5
0.0
−0.5
−1.0
average position
Λ=0
0.0
10.0
20.0
time

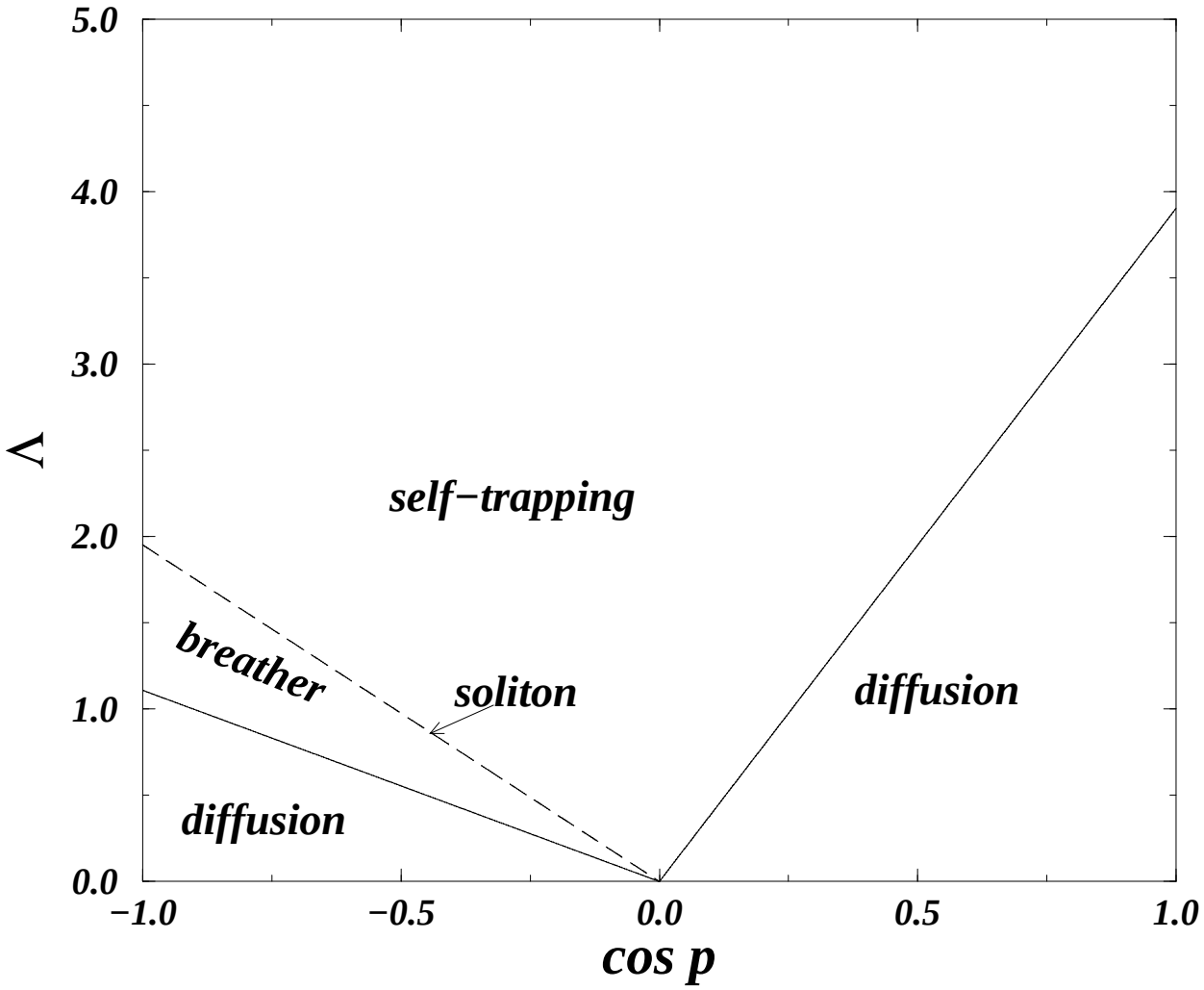
5.0
4.0
3.0
2.0
1.0
0.0
V
self−trapping
breather
soliton
diffusion
diffusion
−1.0
−0.5
0.0
0.5
1.0
cos p

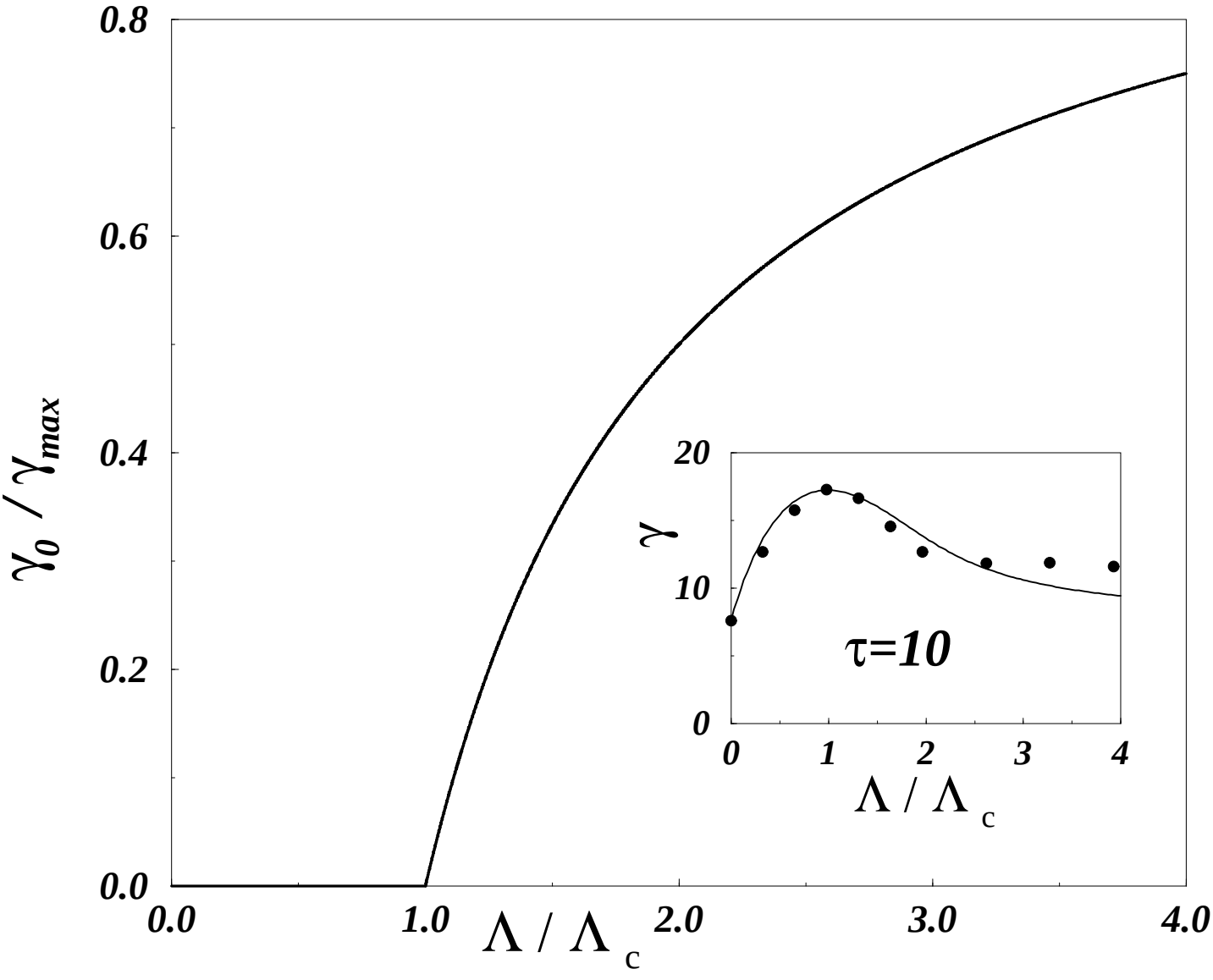
0.8
0.6
0.4
0.2
0.0
γ_0 / γ_{max}
0.0
1.0
2.0
3.0
4.0
Λ / Λ_c
20
10
0
γ
0
1
2
3
4
Λ / Λ_c
τ=10

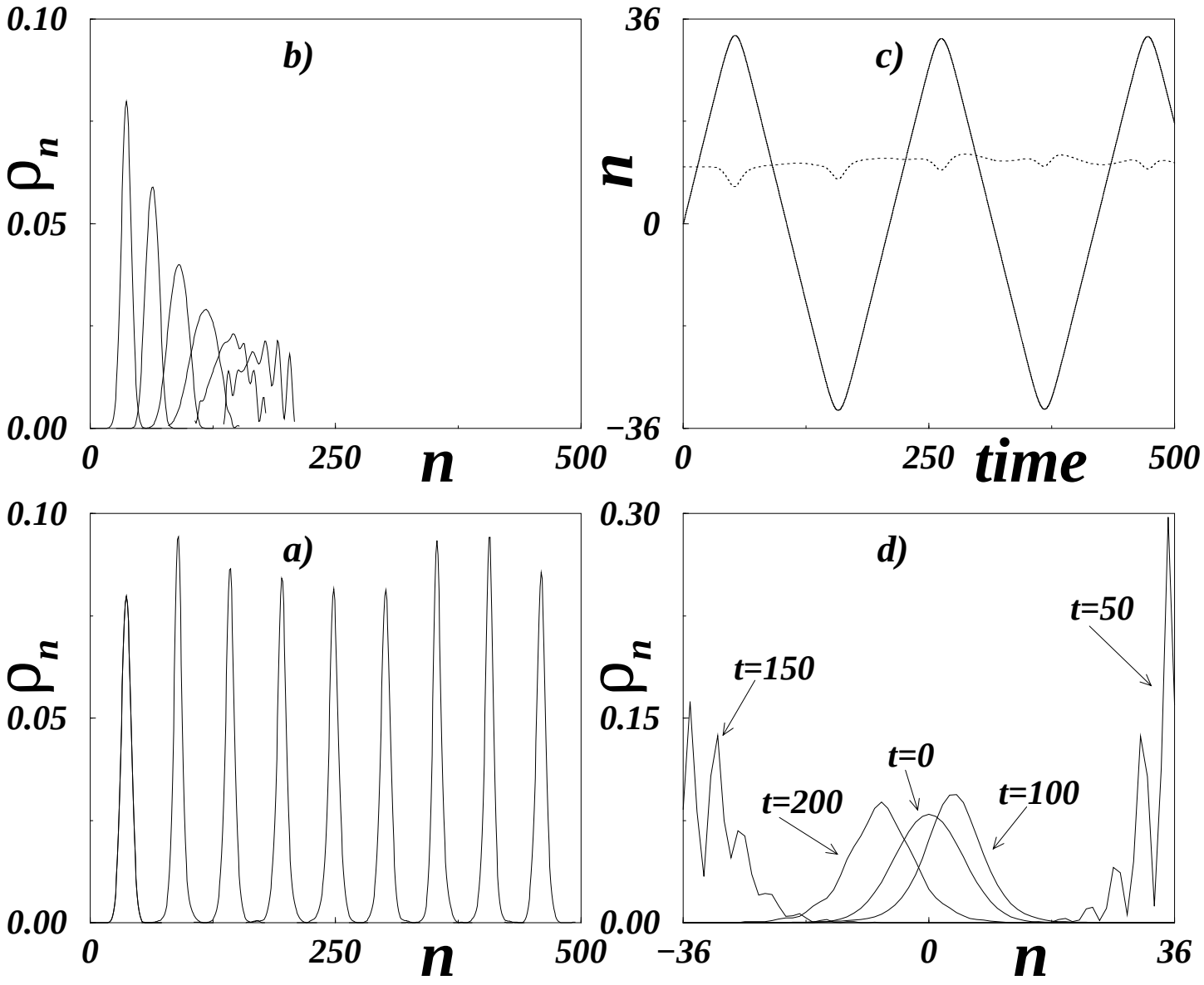
b)
c)
a)
d)
0.10
0.05
0.00
ρ_n
0
250
500
n
36
0
−36
n
time
0.30
0.15
t=50
t=150
t=0
t=100
t=200
−36